Structure of Spheroidal HDL Particles Revealed by Combined Atomistic and Coarse-Grained Simulations

Andrea Catte,*† James C. Patterson,* Denys Bashtovyy,* Martin K. Jones,* Feifei Gu,* Ling Li,* Aldo Rampioni,‡ Durba Sengupta,‡ Timo Vuorela,† Perttu Niemelä,§ Mikko Karttunen,¶ Siewert Jan Marrink,‡ Ilpo Vattulainen,†§‖ and Jere P. Segrest*

*Department of Medicine and Center for Computational and Structural Biology, University of Alabama at Birmingham, Birmingham, Alabama; †Institute of Physics, Tampere University of Technology, Tampere, Finland; ‡Molecular Dynamics Group, Groningen Biomolecular Sciences and Biotechnology Institute, Department of Biophysical Chemistry, University of Groningen, Groningen, The Netherlands; §Laboratory of Physics and Helsinki Institute of Physics, Helsinki University of Technology, Helsinki, Finland; ¶Department of Applied Mathematics, The University of Western Ontario, London, Ontario, Canada; and ‖MEMPHYS Center for Biomembrane Physics, University of Southern Denmark, Odense, Denmark

ABSTRACT Spheroidal high-density lipoprotein (HDL) particles circulating in the blood are formed through an enzymatic process activated by apoA-I, leading to the esterification of cholesterol, which creates a hydrophobic core of cholesteryl ester molecules in the middle of the discoidal phospholipid bilayer. In this study, we investigated the conformation of apoA-I in model spheroidal HDL (ms-HDL) particles using both atomistic and coarse-grained molecular dynamics simulations, which are found to provide consistent results for all HDL properties we studied. The observed small contribution of cholesteryl oleate molecules to the solvent-accessible surface area of the entire ms-HDL particle indicates that palmitoyloleoylphosphatidylcholines and apoA-I molecules cover the hydrophobic core comprised of cholesteryl esters particularly well. The ms-HDL particles are found to form a prolate ellipsoidal shape, with sizes consistent with experimental results. Large rigid domains and low mobility of the protein are seen in all the simulations. Additionally, the average number of contacts of cholesteryl ester molecules with apoA-I residues indicates that cholesteryl esters interact with protein residues mainly through their cholesterol moiety. We propose that the interaction of annular cholesteryl oleate molecules contributes to apoA-I rigidity stabilizing and regulating the structure and function of the ms-HDL particle.

INTRODUCTION

It is well known that in humans, high-density lipoproteins (HDL) are protective against the risk of cardiovascular disease and atherosclerosis (1). Among exchangeable apolipoproteins, the apolipoprotein A-I (apoA-I) is the major protein of plasma HDL and the main carrier of excess cholesterol from peripheral tissues to the liver in a process termed reverse cholesterol transport (RCT) (Fig. 1). In vivo, HDL originates as a pre-β complex of apoA-I and phospholipids that are either secreted intracellularly in the liver and intestine, or are formed extracellularly by the interaction of lipid-poor apoA-I with small amounts of phospholipids. These pre-β HDLs are highly effective acceptors of unesterified cholesterol from cell membranes (2,3).

In the first step of RCT, the ATP-binding cassette transporter A1 (Fig. 1, *ABCA1*) (4) assembles newly synthesized (lipid-poor) apoA-I, phospholipids, and cholesterol to form discoidal HDL particles. During the second step, discoidal HDL particles function as substrates for the activation of the enzyme lecithin:cholesterol acyl transferase (LCAT) (5,6), catalyzed by apoA-I, which is necessary for the esterification of cholesterol molecules in HDL. That process leads to the conversion of cholesterol and phosphatidylcholines to cholesteryl esters and lysophosphatidylcholines. The removal of cholesterol from the surface of these discoidal complexes promotes an important morphological change: the transformation of discoidal HDL into spheroidal HDL. The latter is the form of HDL that circulates in the blood stream. In the third step, spheroidal HDL particles interact with receptors, such as the scavenger receptor type I (SR-BI) (7), leading to cholesterol uptake by the liver and excretion into the bile, remodeling of particles, and regeneration of lipid-free apoA-I.

Remodeling of HDL particles is also performed by other plasma enzymes and transfer proteins, such as the cholesteryl ester transfer protein (CETP) and the phospholipid transfer protein (PLTP). CETP catalyzes the transfer of excess cholesteryl esters from HDL to low-density lipoproteins (LDL) and very-low-density lipoproteins (VLDL) (8). PLTP, on the other hand, promotes the transfer of excess phospholipid molecules from HDL to VLDL, and the conversion of HDL into smaller and larger particles (9,10).

LCAT is a key enzyme in maintaining cholesterol homeostasis and regulating cholesterol transport in the blood stream. In cases of severe LCAT deficiency, cholesterol and cholesteryl esters accumulate in tissues, and the level of unesterified cholesterol increases in blood cells (11,12). Spheroidal HDL
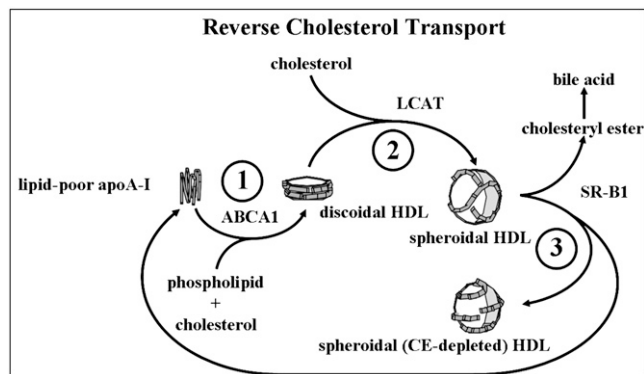
FIGURE 1 Assembly of discoidal and spheroidal HDL in the reverse cholesterol transport.

particles play a significant physiological role in transporting cholesterol from peripheral tissues to the liver for excretion as bile salts, and to steroidogenic tissues for synthesis of steroid hormones. The size of spheroidal complexes is determined primarily by the number of apoA-I and apoA-II molecules per particle. Spheroidal HDL particles containing apoA-I but not apoA-II exhibit two distinct particle sizes with Stokes diameters of 8.5 and 10.8 nm (13), for two and three apoA-I molecules, respectively (14,15). Spheroidal HDL particles containing apoA-I and apoA-II in a 2:1 molar ratio show three distinct particle sizes with Stokes diameters of 8.0, 8.9, and 9.6 nm (13). Spheroidal HDL complexes can also be reconstituted in vitro mainly by means of ultrasound techniques (16).

Although a number of experiments have focused on the structure and dynamics of apoA-I (17) in lipid-free form in solution (18), and in lipid-bound form in discoidal HDL complexes (19,20), the structure and dynamics of apoA-I in spheroidal HDL particles has been elusive. An early study of spherical HDL$_3$ particles proposed that apolipoproteins shared the surface with the polar headgroups of phospholipids (21), whereas cholesteryl esters and triglycerides consituted the hydrophobic core. In spheroidal HDL, the apoA-I amphipathic α-helices probably interact with the acyl chains of lipids (22). This structural view of spheroidal HDL is also similar to that proposed by Hevonoja et al. to describe the structure of spheroidal LDL (23). Sparks and colleagues showed that the structure and stability of apoA-I are a function of particle size for discoidal complexes but not for spheroidal particles (16). Moreover, they found that the valence of apoA-I on in vitro reconstituted spheroidal HDL (r-HDL) is ~1.5 negative charge units less than that for apoA-I on discoidal r-HDL. This result suggests that these two morphological states of HDL may be characterized by different surface charges. Using nuclear magnetic resonance (NMR), the same authors (24) also showed that the apoA-I conformation is sensitive to changes in HDL size and shape.

The above studies, and a more recent surface plasmon resonance study (25), confirm that apoA-I's secondary structure undergoes a significant conformational change during the transition from discoidal to spheroidal HDL. This observation has also been supported by the adaptation of the x-ray crystal structure of Δ43 apoA-I (26) to a model spheroidal HDL in which the enlarged gap between helices 10 of apoA-I should allow the insertion of another apoA-I dimer and, eventually, other apolipoproteins (27). However, studies of the apoA-I structure on discoidal and spherical HDL by fluorescence resonance energy transfer (FRET) (28,29) indicate that the apoA-I registry can also vary.

The structure of apoA-I in discoidal r-HDL particles has also been studied through atomistic molecular dynamics (MD) simulations using the picket fence (30,31) and the double belt (32–34) models. Segrest et al. (30) proposed a double belt model for discoidal HDL. The model consists of lipid-associating domains of apoA-I arranged as continuous antiparallel amphipathic helices around a bilayer disc containing 160 palmitoyloleoylphosphatidylcholine (POPC) molecules to form a 106 Å-diameter particle. Although that model depends upon certain features of the x-ray crystal structure of the lipid-associating domain of apoA-I (26), the general features of the double belt model have been confirmed by different experimental methods (35–37).

Recently, we also showed that in silico the sequential depletion of POPC molecules from a discoidal particle produced dramatic conformational changes in the protein's structure and novel morphologies of HDL particles (38). The particles with POPC/Δ40 apoA-I molar ratios of 100:2 and 50:2 assumed prolate ellipsoidal shapes. These results were confirmed experimentally by Li et al. (37), who used nondenaturing gradient gel electrophoresis (NDGGE) to show that reconstituted discoidal HDL particles containing two apoA-I and variable amounts of dimyristoylphosphatidylcholine (DMPC) molecules, called R2 complexes, display sizes with maximal Stokes diameters of 98 Å (R2-1), 106 Å (R2-2), 110 Å (R2-3), 114 Å (R2-4), and 120 Å (R2-5). They also observed, using NDGGE and negative-stain electron microscopy (EM), that a particle even smaller than the R2-1 particle, a particle of Stokes diameter 78 Å, termed R2-0, results when apoA-I particles are reconstituted in vitro using POPC rather than DMPC (L. Li, J. Chen, F. Gu, J. C. Patterson, A. Catte, and J. P. Segrest, unpublished results). Since the three-dimensional shapes of the 100:2 and 50:2 particles approached a sphere, this result suggests that these two particles could be considered intermediates in the formation of cholesteryl-ester-containing HDL particles with a conformation of apoA-I approximating that in spheroidal circulating HDL. More recently, coarse-grained (CG) MD simulations have also been employed to study the assembly of lipoprotein particles (39,40). Although the structure of the lipoprotein core of cholesteryl esters has been studied by means of atom-scale MD simulations (41), in silico studies of these systems in the presence of apolipoproteins are lacking.

To explore the structure and dynamics of spheroidal HDL particles, we use MD simulations of model spheroidal HDL (ms-HDL) with molar ratios similar to spheroidal r-HDL (16).

Atomistic and CG MD simulations of ms-HDL particles were performed at the physiological temperature (310 K), and also at 410 K. The initial particle, which was previously simulated over 1 ns, with a Δ40 apoA-I double belt surrounding a saddle-shaped POPC bilayer with 80 lipid molecules (38), was subjected to removal of 24 POPC molecules from the center. That was followed by the insertion of a cluster of 16 cholesteryl oleate molecules (CO), generating a starting model with a POPC/CO/Δ40 apoA-I molar ratio of 56:16:2 (Fig. 2). This stoichiometry is representative for subspecies coming from the native HDL$_3$ subclass (42). In both atomistic and CG MD simulations at 310 K, the ms-HDL particles assume prolate ellipsoidal shapes, approaching a spheroidal shape in the all-atom simulation.

The rest of this article is organized as follows. In the next section, we describe the computational details, force fields, and analytical parameters.In Results and Discussion, we perform a comparison of atomistic and CG simulations, and show and discuss the main results. We close this work with a Summary and Conclusions.

MATERIALS AND METHODS

Atomistic force field details

Parameterization of cholesteryl oleate molecules

The initial configuration for a single CO molecule was prepared from co-ordinate files for cholesterol and POPC by working interactively with the molecular modeling program ArgusLab 4.0.1. (43). Using an approach similar to Heikelä et al. (41), the cholesterol molecule was esterified by attaching the oleoyl chain obtained from a POPC molecule to an OH group. In this way, the double bond between C9 and C10 carbon atoms was parameterized using the double-bond region of the oleoyl chain of POPC (Supplementary Material, Fig. S1). The force field for CO molecules was generated from existing CHARMM force fields for cholesterol (44) and POPC (45).

System setup

To prepare the system, we proceeded as follows: first, we generated and simulated a hydrophobic core of CO molecules. Then, we inserted it into a previously simulated model discoidal HDL particle depleted of an adequate number of POPC molecules to allow the insertion of the simulated cluster of CO molecules. Finally, the hydrophobic core was inserted to generate a starting ms-HDL particle. The details of the system setup are described below.

Generation of the CO hydrophobic core

To create a hydrophobic core of CO molecules, a system of 16 CO molecules was built up in a stepwise fashion using the packing of CO molecules in an x-ray crystal structure at 123 K (46) as a reference. First, four isolated molecules were aligned using the Visual Molecular Dynamics (VMD) software to form a starting building block (47). Then it was replicated and four copies of it were aligned. The final structure, containing 16 CO molecules, was subjected to energy minimization first without and then with water. The energy minimization with water was done after solvating the structure with the Solvate plug-in of VMD in a cubic periodic water box extending at least 12 Å beyond every CO molecule. The TIP3P water model was used (48). The system was then simulated for 2 ns using periodic boundary conditions in all directions.

Generation of model spheroidal HDL particles

The starting structure consisted of a previously simulated Δ40 apoA-I double belt surrounding a saddle-shaped POPC bilayer with 80 lipid molecules (38). A total of 24 POPC molecules, half from each monolayer, were removed from the center of the particle. Then, a cluster of 16 CO molecules was inserted to generate a starting model with a POPC/CO/Δ40 apoA-I molar ratio of 56:16:2 (Fig. 2).

Coarse-grained force field details

The atomistic initial structure was coarse-grained using prerelease versions of the MARTINI force field for lipid molecules (49) and of a CG force field for protein molecules (Monticelli, L., S. Kandasamy, X. Periole, R. G. Larson, D. P. Tieleman, and S. J. Marrink, unpublished).

Parameterization of solvent molecules and ions

Four water molecules are represented as a single P-type CG particle. Ions are represented as Q-type CG particles and their first hydration shell is included in the CG representation (49).
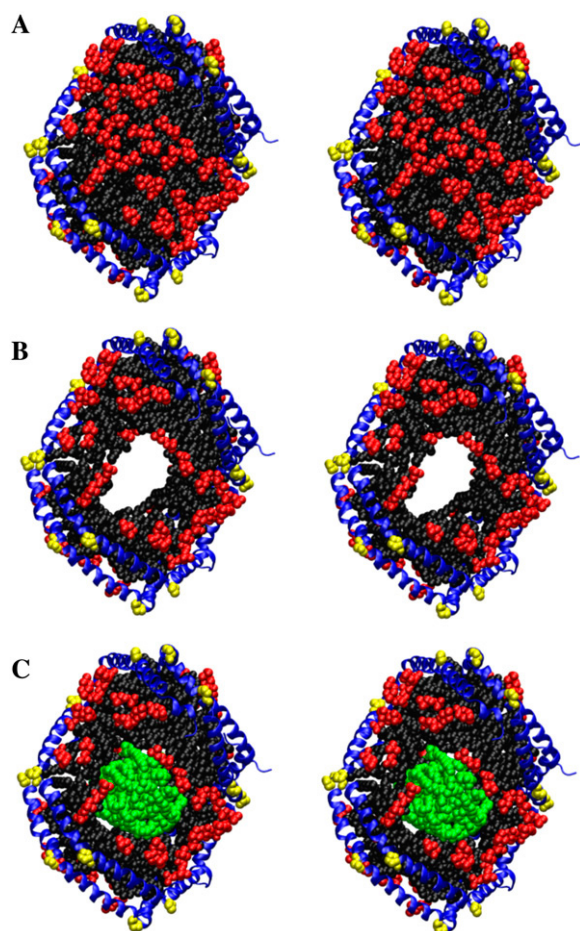

FIGURE 2 Generation of the model spheroidal HDL particle. From top to bottom, the steps for the generation of the model spheroidal HDL initial structure constituted by two Δ40 Apo A-I molecules, 56 POPC lipids, and 16 CO molecules are shown using stereo views of the starting 80:2 particle (*A*), the intermediate 56:2 particle (*B*), and the final model with a POPC:CO:Δ40 apoA-I molar ratio of 56:16:2. ApoA-I molecules are shown as ribbons in blue. POPC molecules are in black for the acyl chains and in red for the polar headgroups. Cholesteryl oleate molecules are shown in green. Prolines are represented in yellow.

Parameterization of cholesteryl oleate molecules

The initial coarse-grained configuration of a single CO molecule was built as follows: the cholesterol moiety of the CO molecule was mapped by eight CG particles using the same approach Marrink et al. employed for cholesterol (49). Then, a standard oleoyl chain was attached to a standard cholesterol moiety, changing the headgroup particle of the cholesterol into a Na-type particle. The detailed parameters of cholesterol and oleoyl CG configurations can be found in the recently published MARTINI force field (49) and in the previous CG force field for lipids (50).

Parameterization of protein molecules

Most amino acids are mapped onto single standard particle types in a way similar to that used recently by other groups (39,51). The mapping chosen in our case reproduces the experimentally determined oil/water partitioning free energy of the amino acid side chain analogs to within 2 kT. The apolar amino acids (Leu, Pro, Ile, Val, Cys, and Met) are represented as C-type particles, the polar uncharged amino acids (Thr, Ser, Asn, and Gln) by the class of P-type particles, and the small negatively charged side chains (Glu and Asp) as Q-type particles. The positively charged amino acids (Arg and Lys) are modeled by a combination of a Q-type and a C-type particle. The bulkier ring-based side chains are modeled by three or four (His, Phe, and Tyr, without or with Trp, respectively) beads of the special class of ring particles. The Gly and Ala residues are only represented by the backbone particle. The type of the backbone particle depends on its secondary structure: when free in solution or in a coil or bend, the backbone has a strong polar character (P-type); as part of a helix or beta-strand, the interbackbone hydrogen bonds reduce the polar character significantly (N-type). The bonded interactions involving amino acid side chains and the peptide backbone were parametrized based on reproducing distributions directly from the protein databank for a large set of membrane proteins. The amount of data is so large that statistically very accurate distributions can be obtained for all the required bonded interactions. Using this procedure, bonded parameters were derived for the backbone (BB) potentials, namely the BB-BB bonded potential, the BB-BB-BB angle potential, and the BB-BB-BB-BB dihedral potential. The last two terms are used to enforce the secondary structure of the backbone, which is therefore an input parameter in the CG model. Different dihedral and angle parameters are used to distinguish a helix, a strand, or a random coil. It is therefore not possible to study realistic folding-unfolding events at this stage. Furthermore, for each amino acid, side-chain (SC) distributions were obtained for the BB-SC bonded potential, the BB-BB-SC angle potential, and the intra-SC potentials for amino acids containing more than one CG particle. Details of the parametrization of the protein force field can be found elsewhere (Monticelli, L., S. Kandasamy, X. Periole, R.G. Larson, D. P. Tieleman, and S. J. Marrink, unpublished).

Simulation protocol

Energy minimization

Each ms-HDL particle was subjected to conjugate gradient energy minimization. Then, the ms-HDL particle was solvated using the Solvate plug-in of VMD (47) in a cubic periodic water cell extending at least 25 Å beyond the lipid headgroups and the protein molecules. To preserve overall charge neutrality and to have physiological ionic strength ($I = 0.15$ M), sodium and chloride ions were placed randomly using the Autoionize plug-in of VMD. The solvated system was then subjected to an additional conjugate gradient energy minimization to reduce steric contacts between the water molecules and the lipoprotein complex. The final model system had ~222,000 atoms (including hydrogens).

Molecular dynamics simulations

Initially, a 10-ns atomistic MD simulation of the ms-HDL particle at 310 K and 1 atm was performed. Both the apoA-I double belt conformation and the packing of lipid molecules changed slightly compared to the starting struc-ture (Supplementary Material, Fig. S2). Then, three different approaches were employed to favor the formation of a better packing of POPC and CO molecules. In the first approach, a 25-ns atomistic MD simulation of the starting model was performed at 310 K and 1 atm. In the second approach, to increase the mobility of POPC molecules for speeding up the coverage of the core of CO molecules, the temperature of the system simulated at 310 K for 10 ns was raised to 410 K without restraints. The resulting structure was subjected to two unrestrained MD simulations of 5 and 10 ns at 410 K and 1 atm.

A temperature higher than the physiological one was also used in the experiments of Sparks et al., who sonicated a mixture of POPC, CO, and apoA-I molecules to reconstitute in vitro spheroidal HDL particles of different sizes (24). After the temperature jump, all ms-HDL particles were cooled down to 310 K, with a velocity reassignment carried out every 1 ps during a 20-ps simulation, and simulated for at least 10 ns at the physiological temperature. After mapping the starting model with CG beads, the third approach involved a long CG simulation of 1 μs at 310 K and 1 atm.

All atomistic MD simulations were performed using NAMD (52). The CHARMM 22 (53,54) and modified CHARMM 27 (45,55) force fields were used for protein and lipid molecules, respectively. Nonbonded van der Waals and electrostatic interactions were truncated using a cutoff distance of 12 Å. We confirmed that the use of truncation did not result in artificial ordering at the truncation distance (Supplementary Material, Figs. S3 and S4). Salt-bridge interactions were treated reliably by the force field in all simulations of ms-HDL particles (56). Velocity reassignment was carried out every 1 ps during the first 30 ps of simulation, increasing the temperature from 30 to 310 K. After that the temperature was kept constant using the Berendsen temperature bath (57). Coordinate trajectories were updated every 10 ps of simulation and all structures were used for analysis. The particle mesh Ewald (PME) (58) treatment of long-range electrostatic interactions was used for all model spheroidal HDL particles. The pressure was held constant at 1 atm for all MD simulations using the Berendsen barostat (57).

CG simulations were performed using GROMACS (59). Prerelease versions of the MARTINI force field and a recently developed CG force field were used for lipid (49) and protein molecules, respectively. The majority of protein residues had α-helical conformation and the remaining residues were in a β-turn conformation.

The final analysis was performed only on the atomistic unrestrained MD simulation at 310 K not subjected to a temperature jump, on atomistic MD simulations at 310 K performed after the temperature jump at 410 K, and on the CG MD simulation at 310 K.

ANALYSIS

Root mean-square deviations

The root mean-square deviations (RMSDs) of protein, POPC, and CO molecules were used to verify the equilibration of each ms-HDL particle. RMSDs of all protein, POPC, and CO molecules were measured over the entire trajectory using the structure obtained after the first 30 ps of the MD simulation as a reference.

We also performed structural alignments of previously simulated model discoidal HDL particles with POPC/Δ40 apoA-I molar ratios of 80:2, 70:2, 60:2, and 50:2 (38) to the ms-HDL particle simulated for 10 ns at 310 K and 10 ns at 410 K using the average position of the α-carbons from the last 20% of each trajectory (Supplementary Material, Fig. S3).

Radius of gyration

The radius of gyration (R_g) of each ms-HDL particle was measured over the entire trajectory and averaged over the last 20% of each trajectory.

Moments of inertia of model spheroidal HDL particles

The moments of inertia were calculated after the alignment of the three principal axes of each system with the x, y, and z directions (60). The components of the moment of inertia of an ellipsoid are given by

$$I_{xx} = \frac{1}{5}M(b^2 + c^2) \quad I_{yy} = \frac{1}{5}M(a^2 + c^2) \quad I_{zz} = \frac{1}{5}M(a^2 + b^2),$$

where M is the total mass of the system and a, b, and c are the semiaxes of an ellipsoid, respectively. In a prolate ellipsoid, a and $b < c$, and in a prolate spheroid $a = b < c$. The principal radii of each ms-HDL were obtained assuming a prolate ellipsoidal shape (61,62).

The components of the moments of inertia of each HDL particle were calculated by averaging every 10 ps during the simulation. The reported results are averages over the last 20% of each trajectory, corresponding to 2 ns and 200 ns for the atomistic and CG simulations, respectively.

Solvent-accessible surface areas

The solvent-accessible surface area (SASA) is used in MD simulations for measuring the extent of the solvent exposure of hydrophobic and hydrophilic domains of the simulated system. It can also be used to detect the timescale needed for readjustment of phospholipids and to check the equilibration of the simulated system.

The SASAs of the ms-HDL particles were measured over the entire trajectory and averaged over the last 20% of each trajectory. Those calculations covered all the atoms, POPC hydrophobic groups, represented by carbon and hydrogen atoms of the fatty acyl chains (palmitoyl and oleoyl chains) without including the carboxyl group, and CO molecules, including all atoms.

Annular CO molecules in model spheroidal HDL particles

Annular CO molecules, defined as those molecules with any atom or bead within 8 Å of any protein atom or bead, were monitored and averaged over the last 40% of each trajectory, corresponding to 4 ns and 400 ns for the atomistic and CG simulations, respectively. A cutoff distance of 8 Å was chosen from the radial distribution function (RDF) of one of the two pairs of carbon atoms of the ester bond region of the CO molecule, namely C^b-C^b (41). That corresponds to the first minimum of the C^b-C^b RDF (see also Supplementary Material). The average number of contacts of three different moieties of the CO molecule (short acyl chain, sterol ring, and oleate chain) with protein residues was also estimated over the last 40% of each trajectory.

Root mean-square fluctuations

The root mean-square fluctuations (RMSFs) of protein α-carbons can give extremely valuable dynamical information by highlighting domains with low and high mobility. RMSFs of protein α-carbons can also provide structural information, detecting different elements of the protein secondary structure.

RMSFs of protein α-carbons were calculated over the last 40% of each trajectory to analyze the flexibility of different helical domains of apoA-I in atomistic and CG ms-HDL complexes.

Interhelical salt bridges

The interhelical salt bridges (ISBs) of the apoA-I double belt were measured over the last 40% of each trajectory of atomistic MD simulations. The oxygen-nitrogen distance cutoff chosen for the calculation was 4 Å. Both buried and exposed ISBs were considered. A buried ISB is formed by residues occupying the helical wheel position 2 (e.g., E111-H155), whereas an exposed ISB is formed by residues in helical wheel positions 5 and 9 (e.g., K96-E169) (34,63,64).

RESULTS AND DISCUSSION

Three approaches for generation of model spheroidal HDL particles

Atomistic MD simulations at 310 K

After performing a short (10-ns) MD simulation of the ms-HDL particle at 310 K, we observed slight changes in the apoA-I conformation and packing of lipid molecules compared to the initial structure (Supplementary Material, Fig. S2). This result is in good agreement with the timescale observed for the formation of phospholipid bilayers (65). Next, we performed a 25-ns MD simulation at 310 K. Despite the longer simulation time, the mutual packing of POPC and CO molecules resulted in good coverage of the hydrophobic core of CO molecules only in some parts of the particle (Fig. 3 *A*). Consequently, we paid more attention to this issue (see below).

Atomistic MD simulations at 310 K and 410 K

To increase diffusion of POPC and CO molecules to speed up the coverage of the core of CO molecules, the structure obtained after the 10-ns simulation at 310 K was subjected to an unrestrained temperature jump to 410 K. Since increased temperatures lead to higher atomic velocities and thus to enhanced molecular motion over a given simulation time, we used the higher temperature as a ''surrogate'' for longer simulation times. Higher temperatures, like longer simulation times, can overcome kinetic energy barriers to lipid diffusion and protein conformational changes. This approach, how-
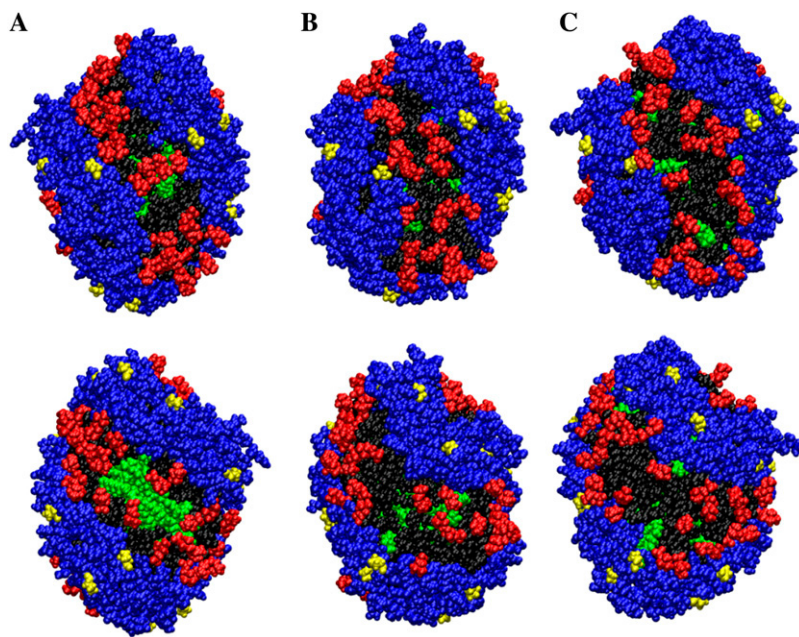
FIGURE 3 Different views (*upper* and *lower*) of the ms-HDL particle constituted by two Δ40 apoA-I molecules, 56 POPC lipids, and 16 CO molecules after MD simulations for 25 ns at 310 K (*A*), 10 ns at 310 K (5 ns at 410 K) (*B*), and 10 ns at 310 K (10 ns at 410 K) (*C*), respectively. The high-temperature simulation affects and improves the packing of POPC and CO molecules even after only 5 ns of MD simulation at 410 K. The exposure to the solvent of the hydrophobic core of CO molecules is reduced compared to the starting model simulated for 10 ns at 310 K. ApoA-I molecules are represented in blue. POPC molecules are in black for the acyl chains and in red for the polar headgroups. Cholesteryl oleate molecules are shown in green, and prolines are in yellow.

ever, comes with a major caveat. Temperature jumps, commonly used in MD-simulated annealing (MDSA) (66), have the distinct possibility of kinetic trapping in energy states other than the global minimum. Since MDSA is used most often in refinement of x-ray and NMR structures (67), constraints are generally placed on the protein to prevent its conformation from drifting too far from the structure under refinement. Our rationale for not applying restraints to either the protein or the lipids is twofold. 1), We hypothesized that the protein surrounding the bilayer in the discoidal HDL particles would add significantly to the stability of the simulated lipoprotein particles in response to temperature jumps. 2), We knew, based upon MD simulations performed on discoidal POPC/apoA-I structures using 20-ns temperature jumps to 500 K, that both the lipid organization and protein structure remain relatively intact under these conditions (data not shown). We therefore reasoned that a more modest jump to 410 K, although acting as a reasonable time ''surrogate'', would have minimal detrimental effects on the overall organization of the lipoprotein particles being simulated. Two sets of simulations at 410 K for 5 and 10 ns were performed, leading to ms-HDL particles with a prolate ellipsoidal shape (Fig. 3, *B* and *C*). Then, both final structures were cooled down to 310 K, as described in the Materials and Methods section, and simulated for another 10 ns.

Coarse-grained MD simulations at 310 K

To monitor the structural and dynamical behavior of the ms-HDL particle over a considerably longer timescale, we also performed a coarse-grained simulation for 1 μs at 310 K using the same initial structure as in atom-scale simulations.

Equilibration of model spheroidal HDL particles

To verify the equilibration of atomistic and CG MD simulation of ms-HDL particles, RMSD values for the protein, POPC, and CO molecules were plotted as a function of time in Figs. 4 and 5, respectively. It is apparent that RMSDs for the ms-HDL particle simulated at 310 K increase rapidly until 1 ns, at which point the rates of change decrease, and then tend gradually to a plateau without reaching equilibrium (Fig. 4 *C*). For ms-HDL particles subjected to MD simulations at 410 K, the observed rapid increase in RMSD, due to the temperature jump, is followed by a plateau, which is reached within a few nanoseconds (Fig. 4, *A* and *B*).

The final structures of all-atom simulations reported in Fig. 3 show that the high-temperature simulation produced an evidently closer packing of POPC and CO molecules (Fig. 3, *B* and *C*) compared to that observed for the ms-HDL particle not subjected to the temperature jump at 410 K (Fig. 3 *A*). It is also worth noting that the temperature jump influenced the phase behavior of CO molecules, but not that of POPC molecules, as shown by RDF results for different pairs of atoms (Supplementary Material, Figs. S4 and S5). The RMSD plot of the CG ms-HDL particle shows a marked increase, for POPC and CO molecules, to 200 ns, whereas protein molecules reach a plateau within essentially the same time frame (Fig. 5). After 200 ns, all components except for POPC molecules of the CG model are found to be equilibrated.

On the basis of the above findings, the following analysis and discussion will mainly focus on equilibrated atomistic and CG structures simulated for 10 ns at 310 K and 10 ns at 410 K, and for 1 μs at 310 K, respectively.
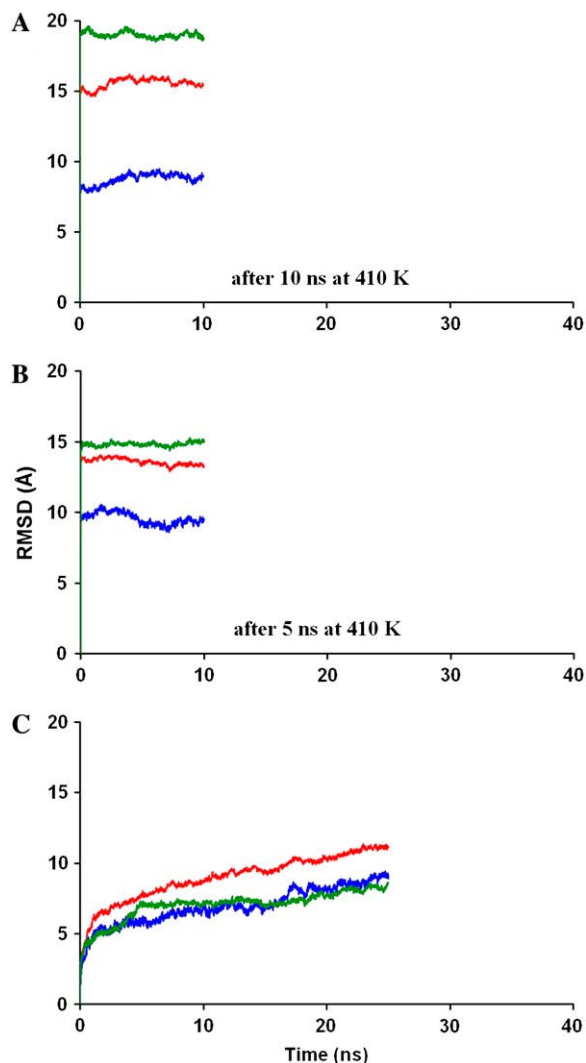
FIGURE 4 RMSD values of apoA-I (*blue*), POPC (*red*), and CO (*green*) molecules for atomistic MD simulations performed for 10 ns at 310 K (10 ns at 410 K (*A*) and 5 ns at 410 K (*B*), respectively) and for 25 ns at 310 K (*C*). RMSD values of all components show that only the ms-HDL structure subjected to the longer MD simulation at 410 K reaches the equilibration after 5 ns.

Model spheroidal HDL particles assume a prolate ellipsoidal shape

Different views of atomistic and CG particles simulated at 310 K are shown in Fig. 6. Both simulated structures are characterized by a prolate ellipsoidal or spheroidal shape (Fig. 6, *A* and *B*) with an average major diameter of 84 Å and a radius of gyration of ~28 Å. These are in good agreement with experimental values of 76 ± 5 Å (from NDGGE measurements) and 74 ± 15 Å (from EM measurements) for the major diameter reported by Sparks et al. (16).

The presence of a prolate ellipsoidal shape was also confirmed by the results computed for the moments of inertia. The values obtained were employed to calculate the semiaxes of each particle reported in Table 1. In atomistic models, the
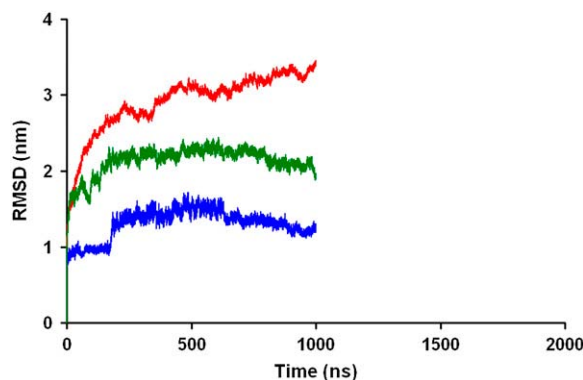
FIGURE 5 RMSD values of apoA-I (*blue*), POPC (*red*), and CO (*green*) molecules for coarse-grained MD simulations performed for 1 μs at 310 K. RMSD values of all components show that the CG ms-HDL structure reaches equilibrium after ~200 ns.

values of the minor semiaxes are very similar to each other (ranging from 30 to 35 Å) and smaller than the major semiaxis (average value of 43 Å), indicating that the structure is approaching a prolate spheroid shape. The CG model showed also a prolate ellipsoidal shape with a major principal radius of 46.5 ± 0.8 Å, in good agreement with the atomistic result (42.9 ± 0.4 Å), whereas minor semiaxes were found to be somewhat smaller ($a = 26.4 \pm 0.9$ Å) and larger ($b = 39.8 \pm 1.3$ Å) than atomistic results ($a = 31.0 \pm 0.3$ Å and $b = 35.2 \pm 0.3$ Å), respectively. Here, there is reason to stress the substantially larger timescale of CG simulations, though: when we started the CG simulation of an initial structure that was essentially identical to the one used in atomistic simulations, and simulated the CG system for a short period of 2.5 ns, we found results identical to those in the atomistic model. Further, as Fig. 5 shows that the equilibration of these complex particles takes on the order of several hundred nanoseconds, the minor differences between atomistic and CG model results are not surprising. Considering the fact that the CG model is simulated over 1000 ns compared to the 10-ns period in the atomistic model, it is perhaps more surprising to find that differences are so minor indeed. The 410 K temperature jump perhaps explains a portion of the similarity between the two types of simulated structures.

Solvent-accessible surface area of model spheroidal HDL particles

The SASA of atomistic and CG ms-HDL particles for the entire ms-HDL particle, POPC hydrophobic chain groups, and all CO molecules are shown in Table 2. The SASA of the entire ms-HDL particle was found to remain almost unchanged, each average value being within the standard deviation. This indicates that although there was a tendency toward a lower value, the total exposure to the solvent was not greatly affected by the temperature jump. Overall, this result shows that the average solvation free energy is constant
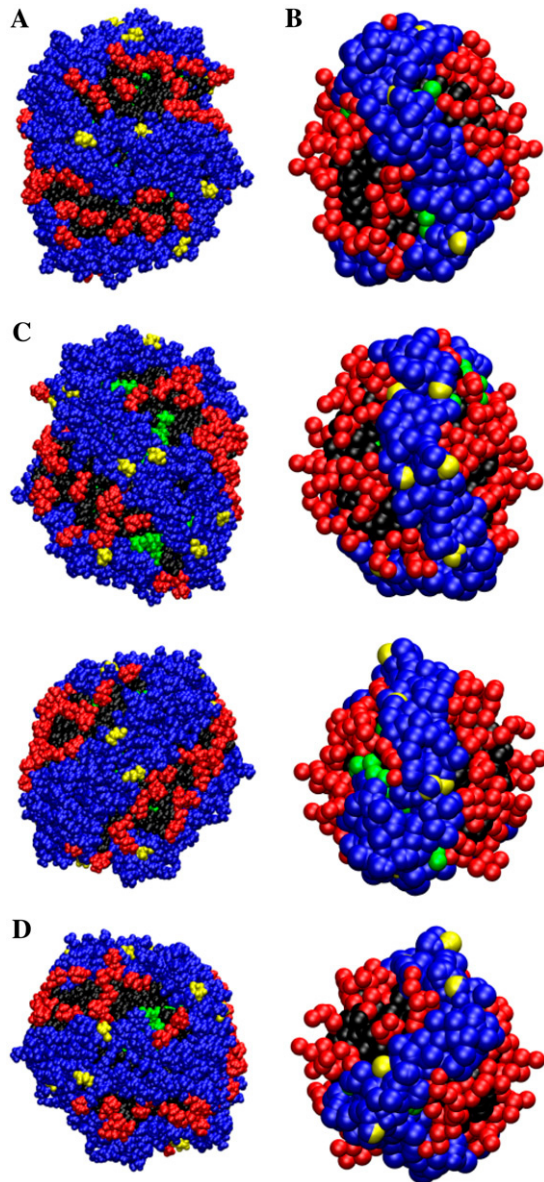
FIGURE 6 Different rotational views of atomistic and CG ms-HDL particles simulated at 310 K for 10 ns (after being simulated at 410 K for 10 ns) (*A*) and 1 μs (*B*), respectively. Both simulated structures are characterized by a prolate ellipsoidal shape with an average long diameter of 84 Å and an average radius of gyration of 28 Å. Two of the three pseudo-C2 axes of symmetry, which are oriented perpendicular to each other, are also shown with the correspondent 180°-rotated structures (*C* and *D*). The same color code was used as in Fig. 3.

TABLE 1 Components of the moments of inertia (*I*) and values of semiaxes (*a*–*c*) of ms-HDL particles from atomistic and CG MD simulations

	Particle	
I (kg/Å^2/10^{-3})*	10 ns at 310 K	
a, b, and c (Å)*	(10 ns at 410 K)	1 μs at 310 K
I_{xx}	61.1 ± 0.6	23.3 ± 0.8[†]
I_{yy}	55.6 ± 0.6	17.8 ± 0.4[†]
I_{zz}	43.5 ± 0.5	14.2 ± 0.4[†]
a	31.0 ± 0.3	26.4 ± 0.9
b	35.2 ± 0.3	39.8 ± 1.3
c	42.9 ± 0.4	46.5 ± 0.8

*All atoms or beads of each ms-HDL particle were included in the calculation and all values were averaged over the last 20% of the trajectory.
[†]The components of the moment of inertia of the CG model are smaller than those of the atomistic model, because the total mass of the CG model is smaller than the corresponding total mass of the atomistic model. What is relevant here is to compare the relative magnitudes of the different inertia tensor components.

average value of ~49 Å^2 per POPC (SD ~ 3 Å^2) for the ms-HDL particle not subjected to a temperature jump, indicating that the packing of POPC molecules is as good as in our previous model HDL complexes, in which this value ranged from 47 Å^2 to 50 Å^2 (38). In ms-HDL particles subjected to a temperature jump to 410 K, the average SASA of POPC hydrophobic chains/POPC is ~52 Å^2 (SD ~ 3 Å^2), which is also in good agreement with our previous results.

The fact that all simulated systems are characterized by a reasonably good packing of protein and lipid molecules is supported by the analysis of the SASA of CO molecules. Their contribution to the total SASA of the entire ms-HDL particle is <2% for all three simulations, and decreases more markedly in the ms-HDL particles that were subjected to a temperature jump. This result shows that the protein and POPC molecules do very well in terms of covering the hydrophobic core of CO molecules, and that the longer the simulation time at 410 K, the better the overall packing of POPC, CO, and protein molecules. In this respect, it is worth pointing out that in the CG model, the SASAs of the entire HDL particle and POPC hydrophobic chain groups are smaller than the values observed in atomistic models. This is fully understandable due to the coarse-grained nature of the model: if several atom-scale groups are mapped together in a manner where the interactions in the CG description are described in a spherical fashion, the solvent accessible surface area evidently is decreased compared with the atomistic description. This implies that it is not reasonable to compare the quantitative SASA values given by the atomistic and CG models. Rather, one should focus on the trends predicted by the two descriptions. In this respect, the atom-scale and CG models are fully consistent with one another and highlight the substantial coverage of the hydrophobic core comprised of cholesteryl oleate molecules. Moreover, what is also in favor of our studies for both atomistic and CG models is the fact that the contribution of the SASA of all CO molecules to the

for all three ms-HDL particles. Moreover, it is also worth noting that the packing of POPC molecules was slightly better in the ms-HDL particle not subjected to a temperature jump

The SASA values obtained for the POPC hydrophobic chain groups are very similar to those reported in the literature by Klon et al. (32). This result is probably due to the movement of CO molecules toward the protein and away from the bilayer. The SASA of POPC acyl chains reaches an

TABLE 2   SASA (Å²) of ms-HDL particles from atomistic and CG MD simulations

Particle SASA (Å²)	25 ns	10 ns (5 ns at 410 K)	10 ns (10 ns at 410 K)	1 μs at 310 K
$SASA_{ms\text{-}HDL}^{*}$	36415 ± 503	36390 ± 360	36172 ± 456	27501 ± 517
$SASA_{POPC}^{\dagger}$	2721 ± 158	2936 ± 159	2916 ± 142	923 ± 191
$SASA_{CO}^{\ddagger}$	678 ± 83	656 ± 72	569 ± 87	197 ± 98

Columns 1–3 are for an atomistic model and column 4 is for CG model. See text for details of the comparison. All SASA values were averaged over the last 20% of each trajectory.

*All atoms of each ms-HDL particle were included in the calculation.

†Only the atoms of POPC hydrophobic chain groups, defined as in a previous work (38), were used for computing this parameter.

‡All atoms of CO molecules were accounted for.

total SASA of the entire ms-HDL particle is <1%, suggesting that ms-HDL particles subjected to high-temperature simulations are consistent with the result achieved in the longer timescale of the CG simulation at a lower temperature.

Annular shell of CO molecules in model spheroidal HDL particles

Annular CO molecules (defined above) of the atomistic and CG models are shown in Fig. 7. It is remarkable that all CO molecules are within the chosen cutoff distance in the atomistic simulation. Also in the CG simulation, the majority (75%) of CO molecules can be considered annular, suggesting that the intercalation of CO molecules with protein residues could play an important structural role in the stability of spheroidal HDL particles (Fig. 7, *upper row*, and Supplementary Material, Fig. S6).

The hydrophobic core of CO molecules, represented by those atoms or beads that are not within the chosen cutoff of 8 Å of any protein atom or bead, remains stable for all atomistic
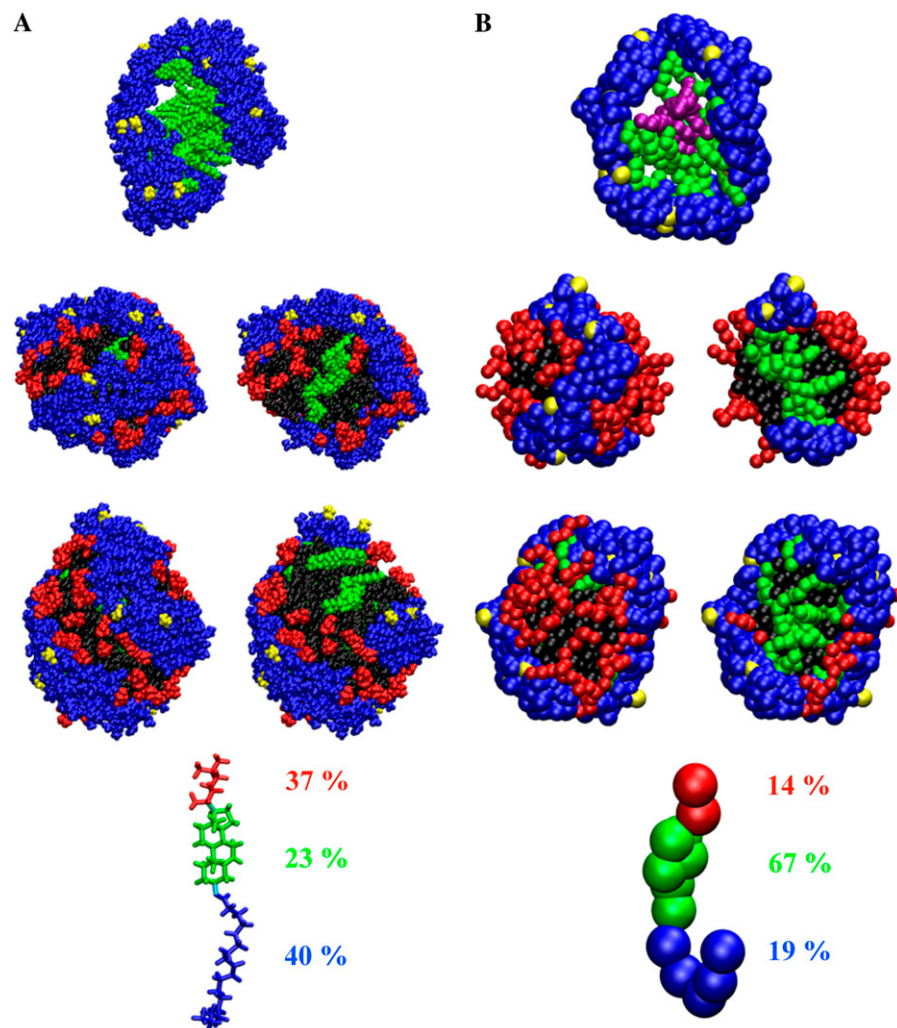

FIGURE 7   Annular shell of CO molecules and packing of the hydrophobic core of CO molecules with POPC and apoA-I molecules. (*Upper row*) Annular CO molecules, defined as those molecules within 8 Å of any protein atoms or beads, are shown in green for the ms-HDL particle simulated for 10 ns at 310 K (after 10 ns at 410 K) (*A*) and for the CG ms-HDL particle simulated for 1 μs at 310 K (*B*), respectively. ApoA-I molecules are in blue. Proline residues are in yellow. Central CO molecules were observed only in the structure not subjected to the temperature jump (Supplementary Material, Fig. S6) and in the CG model (*B*) in purple. (*Middle rows*) The packing of CO molecules in atomistic and CG ms-HDL particles shows the interdigitation and intercalation of CO molecules with POPC and apoA-I molecules, respectively. (*Lower row*) Licorice and bead representations of the atomistic and CG CO molecule with its different moieties highlighted in red (short acyl chain), green (sterol ring), and blue (oleate chain). The percentage of the average number of contacts of different parts of the CO molecule is also shown, with the same color code as that used to represent the different moieties of the CO molecule.

structures and for the coarse-grained model (Supplementary Material, Fig. S9). The analysis of the trajectory of the CG simulation suggests that the motion of CO molecules toward the protein is probably characterized by a dynamic equilibrium in which the fast exchange between annular and central CO molecules contributes to the stability of the hydrophobic core of CO molecules (Supplementary Material, Fig. S10 and Movie 1).

The packing of the hydrophobic core of CO molecules is also characterized by the intercalation of CO molecules with protein residues, and the interdigitation of CO molecules with POPC molecules (Fig. 7, *middle rows*). The analysis of the fraction of the average number of contacts of different moieties of the CO molecule within 8 Å of protein residues (Fig. 7, *lower row*) points out that in the atomistic model, the oleate chain (40%) moiety interacts less with protein residues than the cholesterol moiety (sterol ring (23%) and the short acyl chain (37%)). A similar result is also observed in the CG simulation, in which the oleate chain (19%) moiety shows even less interaction with protein residues than the cholesterol moiety of CO (sterol ring (67%) and short acyl chain (14%)).

Secondary structure of apoA-I molecules in model spheroidal HDL particles

The protein secondary structure of the model spheroidal HDL particle not subjected to a temperature jump and simulated for 25 ns is mainly α-helical and punctuated with a few β-turns and random coil domains (Supplementary Material, Fig. S6). Although a long simulation at 410 K speeds up the process of getting a better packing of POPC and CO molecules, it also affects the secondary structure of the protein.

As shown in Fig. 7 (see Supplementary Material, Fig. S5, for more details), the particle simulated first for 10 ns at 310 K and then for 10 ns at 410 K shows more extended β-turns in the protein structure in two different chains (residues 47–59 and residues 63–80 in chain B, and residues 197–219 in chain A), a small 3- to 10-helix region (residues 60–62 in chain B), and even two small π-helices (residues 42–46 and residues 235–239 in chain B). The observed π-helical conformations displayed average ϕ/ψ angles of $(-74, -52)$ for residues 42–46 and $(-73, -58)$ for residues 235–239, with an average standard deviation of 4° (averages over the last 40% of the trajectory). These values are much closer to the values of $(-75, -60)$, commonly observed in simulations, than to the experimental values of $(-76, -41)$. This indicates that the formation of this structural motif was possibly force-field-dependent, as previously reported by Feig et al. (68).

However, similar structural changes were not observed in the structure subjected to a 5-ns simulation at 410 K (Supplementary Material, Fig. S6), suggesting that the temperature-jump procedure could be calibrated to get a protein secondary structure similar to that observed experimentally. In fact, the secondary structure analysis performed by Sparks and colleagues (16) estimated the presence of β-turns and β-sheet

regions in their reconstituted spheroidal HDL particle and also predicted random coil domains punctuating the amphipathic α-helical structure of apoA-I (24).

Comparison of protein fluctuations from RMSFs of protein α-carbons

The α-helical structure of the protein exhibits very little mobility for all atomistic ms-HDL particles and also for some domains of the CG ms-HDL particle. This view is summarized in the RMSF data of protein α-carbons reported in Fig. 8. The very small difference in flexibility among the two protein chains is also noteworthy. The protein stays rigid, perhaps to simply lend stability to the overall structure. The protein tertiary structure does not change dramatically compared to that in our previous ellipsoidal model HDL particles (Supplementary Material, Fig. S3). The peaks are most often representative of unstructured regions connecting secondary structure (69), and the majority of them mainly correspond to turns in α-helices that point away from the protein into the solvent.

A good example of the above is the atomistic model that was not subjected to a temperature jump (Supplementary Material, Fig. S7). In that model, alanine residue 187 of chain B belongs to a turn region of the protein and to a structural motif GLY-GLY-ALA that connects two α-helical domains in helices 7 and 8. In the same atomistic model in chain A,
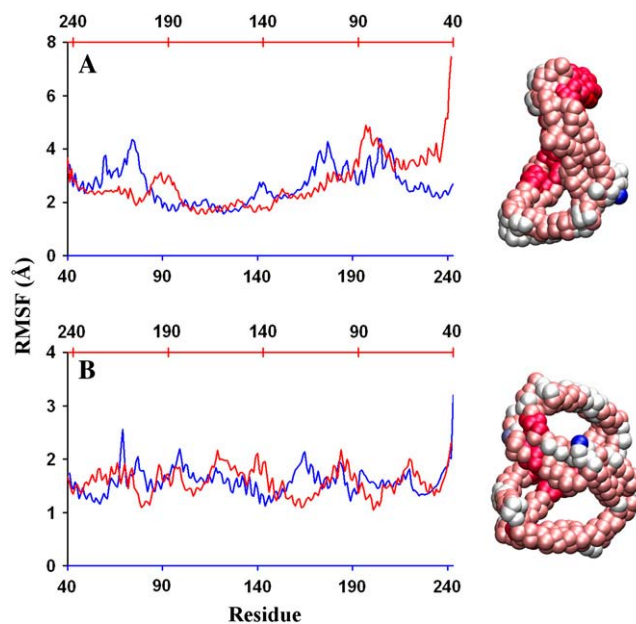
FIGURE 8 Root mean-square fluctuation profiles for apoA-I α-carbons (*blue*, chain A; *red*, chain B) shown for the CG simulation performed at 310 K for 1 μs (A) and the atomistic MD simulation performed at 310 K for 10 ns (10 ns at 410 K) (B), respectively. The α-carbons are also shown, with different-colored beads for both CG and atomistic structures to stress more rigid (*red*) and more flexible (*blue*) domains of the protein structure (see also Supplementary Material, Fig. S9).

leucine residue 219 of helix 9 is in a random coil conformation, connecting two α-helical domains in helices 9 and 10. These peaks are usually observed in residues of the N-terminus and C-terminus of the protein. However, the most meaningful interpretation of the data is obtained by examining the trends and relative flexibilities among different regions of the protein dictated by the temperature jump. The protein with structures subjected to an intermediate simulation step at 410 K becomes increasingly rigid with longer simulation times at 410 K (Supplementary Material, Fig. S7). In particular, this feature is found in the most flexible regions observed in the simulation of the system not subjected to the temperature jump (Supplementary Material, Fig. S7).

It is worth noting that even in the longer timescale used in the CG simulation, there are still extended rigid domains and more flexibility due to the increased sampling (Fig. 8 A). The observed rigidity is probably a dramatic consequence of the intercalation of CO molecules with some protein residues (70). A similar interaction among cholesterol molecules and protein residues was also proposed by Sparks et al. (71) to explain the contrasting changes on the surface charge of apoA-I containing reconstituted discoidal HDL complexes upon addition of increasing amounts of unesterified cholesterol molecules. Since cholesterol molecules affect both the order of POPC molecules and the stability of apoA-I molecules in discoidal complexes, CO molecules might have a greater effect on protein stability than on the orientation order of POPC molecules in spheroidal HDL particles.

These results are also in good agreement with RMSD data of the structural alignments to the protein of model discoidal HDL particles with a prolate ellipsoidal shape (38) (Sup-

plementary Material, Fig. S3), which explains why the majority of the domains of the protein are rigid, suggesting that a small apoA-I conformational change might be required to accommodate a CO hydrophobic core in prolate ellipsoidal HDL particles.

Interhelical salt bridges in atomistic-model spheroidal HDL particles

Interhelical salt bridges of atomistic ms-HDL particles, measured as described in Materials and Methods, are shown in Table 3. The temperature jump did not have a marked effect on the total number of ISBs. Although the high-temperature simulation induced the loss of some salt bridges, it is remarkable that their overall number increased in structures subjected to MD simulations at 410 K, reaching the maximum value of 19. This increase in ISBs might also contribute to the rigidity of the protein as shown by RMSF data (Fig. 8). Two buried ISBs, D89-R177 and E111-H155, are present in all three atomistic models. Although the buried ISB E78-R188 is formed only by glutamic acid in position 78 of chain B and arginine in position 188 of chain A, it is lost in the structure subjected to a 10-ns MD simulation at 410 K (Table 3).

Among the remaining exposed ISBs, there is reason to notice the conservation of salt bridges between residues in helices 3 and 7 (E92-R173 and K96-E169), and helices 5 and 5 (E125-K140 and E125-K133). The contribution of these salt-bridge interactions to the overall stability of apoA-I in spheroidal HDL particles might be important. This has been recently observed in discoidal HDL particles as well (72). In addition, we observed an interesting promiscuous salt bridge

TABLE 3 Interhelical salt bridges

Helix pairs*	Particle		
	25 ns	10 ns (5 ns at 410 K)	10 ns (10 ns at 410 K)
1 (residues 43–65) 9 (residues 209–219)	K 45 B–D 213 A	K 45 A–D 213 B	/
2 (residues 66–87)		E 70 B–K 206 A	E 70 B–K 206 A
8 (residues 187–208)	E 70 A–K 195 B E 70 B–H 199 A E 78 B–R 188 A	K 77 A–E 191 B E 78 A–K 195 B E 78 B–R 188 A E 85 A–R 188 B	E 70 A–H 199 B K 77 A–E 191 B E 78 A–K 195 B E 78 B–H 199 A E 85 A–R 188 B
3 (residues 88–98)	D 89–R 177[†]	D 89–R 177[†]	D 89–R 177[†]
7 (residues 165–186)	E 92 A–R 173 B K 96 B–E 169 A	E 92 B–R 173 A K 96–E 169[†]	E 92–R 173[†] K 96–E 169[†]
4 (residues 99–120) 6 (residues 143–164)	E 111–H 155[†]	E 111–H 155[†]	E 111–H 155 [a]
5 (residues 121–142) 5 (residues 121–142)	E 125 B–K 133 A E 125 B–K 140 A	E 125 B–K 133 A E 125 B–K 140 A	E 125–K 133[†] E 125–K 140[†] E 128 B–K 133 A

*All interhelical salt bridges were within the 4-Å cutoff over the last 40% of each trajectory.
[†]Salt bridges were formed on both chains.

formed by glutamic acid in position 125 of chain B with two lysines, in positions 133 and 140, respectively. The same salt bridge was reported by Klon et al. (32), and its ''survival'' during the temperature jump probably means that it has an important structural role in spheroidal HDL particles as well.

CONCLUSIONS

The esterification of the cholesterol molecules of discoidal HDL, operated by LCAT (5,6), an enzyme activated by apoA-I, plays an important physiological role in the transition from the nascent form of discoidal HDL to its spheroidal form circulating in the blood. This important morphological change is characterized by the removal of unesterified cholesterol from the surface of discoidal HDL through the phase separation of cholesteryl esters, creating the hydrophobic core of spheroidal HDL. To better understand the structure and dynamics of the protein and lipid components at atomic and molecular scales, we performed atomistic and coarse-grained MD simulations for a model spheroidal HDL particle containing a core of cholesteryl oleate molecules.

Both atomistic and CG MD simulations give equilibrated protein-lipid structures that are consistent with experimental results: the three-dimensional shapes of both atomistic and CG ms-HDL particles shown in Fig. 6 are prolate ellipsoidal, approaching a prolate spheroid shape in the atomistic case, with sizes comparable to in vitro reconstituted spheroidal HDL particles (16,24). The solvent-accessible surface area of all ms-HDL particles remains constant within error, suggesting that all systems converge to an average structure. The SASA of POPC hydrophobic acyl chains/POPC is comparable to the values reported in our previous work (38), indicating that the packing of POPC molecules is as good as in model discoidal HDL complexes. Furthermore, the small contribution of the SASA of CO molecules to the total SASA of our systems stresses that the apoA-I double belt and POPC molecules do a good job in covering the hydrophobic core of CO molecules. These results suggest that the conformation of apoA-I in these models might approximate the conformation of apoA-I in spheroidal circulating HDL.

The diffusion coefficients of CO molecules determined through atom-scale simulations are found to be of the same order of magnitude as in a previously published atomistic simulation study of the core of lipoprotein particles (41). Moreover, the radial distribution functions of POPC and CO molecules in the atomistic models are also found to be in agreement with the corresponding results of the CG model (see Supplementary Material). The phase behavior of POPC molecules is unaffected by the temperature jump to 410 K and remains essentially the same even on the longer timescale of the CG simulation. However, the temperature jump to 410 K exerts a major effect on the phase behavior of CO molecules. The longer the simulation time at 410 K, the more dramatically altered is the short-range order of CO molecules. The high-temperature simulation disrupts the ordering of bulk CO

molecules and favors their movement toward the protein, bringing the population of annular CO molecules of atomistic and CG models to its maximum value, as shown in Fig. 7. The analysis of the fraction of the average number of contacts of different moieties of the CO molecule with protein residues indicates that CO molecules interact with apoA-I molecules mainly in their cholesterol moiety.

Furthermore, the combined effect of a simultaneous intercalation of CO molecules with protein residues (71), as highlighted by the large number of annular CO molecules shown in Fig. 7 and by RMSFs of the protein α-carbons reported in Fig. 8, might also affect the orientation order of POPC molecules. These results suggest that the intercalation of CO molecules with protein residues might play an important structural role and contribute actively to the stability and function (e.g., the biological activities of the enzyme, LCAT, and the exchange protein, CETP) of spheroidal HDL particles.

Ultrasound (16) and enzymatic methods (73) can be used to produce spheroidal HDL particles that can be studied with different experimental techniques, such as NMR, x-ray diffraction, fluorescence resonance energy transfer, and cryoelectron microscopy, to test features of present and future atomistic and coarse-grained models of spheroidal HDL. Our models provide important insights for future research to investigate the structure and function of spheroidal HDL at a molecular level to gain understanding of the conformational changes undergone by apoA-I during the transition from discoidal HDL to spheroidal HDL; the biological implications of the interaction among cholesteryl esters, the protein, and phospholipid molecules; and the structural role of LCAT in the assembly of spheroidal HDL.

SUPPLEMENTARY MATERIAL

To view all of the supplemental files associated with this article, visit www.biophysj.org.

REFERENCES

1. Linsel-Nitschke, P., and A. R. Tall. 2005. HDL as a target in the treatment of atherosclerotic cardiovascular disease. *Nat. Rev. Drug Discov.* 4:193–205.

2. Rye, K. A., and P. J. Barter. 2004. Formation and metabolism of prebeta-migrating, lipid-poor apolipoprotein A-I. *Arterioscler. Thromb. Vasc. Biol.* 24:421–428.

3. Rye, K. A., M. Duong, M. K. Psaltis, L. K. Curtiss, D. J. Bonnet, R. Stocker, and P. J. Barter. 2002. Evidence that phospholipids play a key

role in pre-β apoA-I formation and high-density lipoprotein remodeling. *Biochemistry*. 41:12538–12545.

4. Oram, J. F., and J. W. Heinecke. 2005. ATP-binding cassette transporter A1: a cell cholesterol exporter that protects against cardiovascular disease. *Physiol. Rev.* 85:1343–1372.

5. Jonas, A. 2000. Lecithin cholesterol acyltransferase. *Biochim. Biophys. Acta*. 1529:245–256.

6. Peelman, F., N. Vinaimont, A. Verhee, B. Vanloo, J. L. Verschelde, C. Labeur, S. Seguret-Mace, N. Duverger, G. Hutchinson, J. Vandekerckhove, J. Tavernier, and M. Rosseneu. 1998. A proposed architecture for lecithin cholesterol acyl transferase (LCAT): identification of the catalytic triad and molecular modeling. *Protein Sci.* 7:587–599.

7. Trigatti, B. L., M. Krieger, and A. Rigotti. 2003. Influence of the HDL receptor SR-BI on lipoprotein metabolism and atherosclerosis. *Arterioscler. Thromb. Vasc. Biol.* 23:1732–1738.

8. Rye, K. A., N. J. Hime, and P. J. Barter. 1997. Evidence that cholesteryl ester transfer protein-mediated reductions in reconstituted high density lipoprotein size involve particle fusion. *J. Biol. Chem.* 272:3953–3960.

9. Rye, K. A., M. Jauhiainen, P. J. Barter, and C. Ehnholm. 1998. Triglyceride-enrichment of high density lipoproteins enhances their remodelling by phospholipid transfer protein. *J. Lipid Res.* 39:613–622.

10. Huuskonen, J., V. M. Olkkonen, M. Jauhiainen, and C. Ehnholm. 2001. The impact of phospholipid transfer protein (PLTP) on HDL metabolism. *Atherosclerosis*. 155:269–281.

11. Castro, G. R., and J. C. Fielding. 1988. Early incorporation of cell-derived cholesterol into prebeta-migrating high density lipoprotein. *Biochemistry*. 27:25–29.

12. Kuivenhoven, J. A., H. Pritchard, J. Hill, J. Frohlich, G. Assmann, and J. Kastelein. 1997. The molecular pathology of lecithin: cholesterol acyltransferase (LCAT) deficiency syndromes. *J. Lipid Res.* 38:191–205.

13. Cheung, M. C., and J. J. Albers. 1984. Characterization of lipoprotein particles isolated by immunoaffinity chromatography: particles containing A-I and A-II and particles containing A-I but no A-II. *J. Biol. Chem.* 259:12201–12209.

14. Rye, K. A., M. A. Clay, and P. J. Barter. 1999. Remodelling of high density lipoproteins by plasma factors. *Atherosclerosis*. 145:227–238.

15. Rye, K. A., and M. Duong. 2000. Influence of phospholipid depletion on the size, structure, and remodeling of reconstituted high density lipoproteins. *J. Lipid Res.* 41:1640–1650.

16. Sparks, D. L., S. Lund-Katz, and M. C. Phillips. 1992. The charge and structural stability of apolipoprotein A-I in discoidal and spherical recombinant high density lipoprotein particles. *J. Biol. Chem.* 267:25839–25847.

17. Gursky, O. 2005. Apolipoprotein structure and dynamics. *Curr. Opin. Lipidol.* 16:287–294.

18. Silva, R. A. G. D., G. M. Hilliard, J. Fang, S. Macha, and W. S. Davidson. 2005. A three-dimensional molecular model of lipid-free apolipoprotein A-I determined by cross-linking/mass spectrometry and sequence threading. *Biochemistry*. 44:2759–2769.

19. Davidson, W. S., and R. A. G. D. Silva. 2005. Apolipoprotein structural organization in high density lipoproteins: belts, bundles, hinges and hairpins. *Curr. Opin. Lipidol.* 16:295–300.

20. Saito, H., P. Dhanasekaran, D. Nguyen, E. Deridder, P. Holvoet, S. Lund-Katz, and M. C. Phillips. 2004. Alpha-helix formation is required for high affinity binding of human apolipoprotein A-I to lipids. *J. Biol. Chem.* 279:20974–20981.

21. Edelstein, C., F. J. Kezdy, A. M. Scanu, and B. W. Shen. 1979. Apolipoproteins and the structural organization of plasma lipoproteins: human plasma high density lipoprotein-3. *J. Lipid Res.* 20:143–153.

22. Mishra, V. K., M. N. Palgunachari, J. P. Segrest, and G. M. Anantharamaiah. 1994. Interactions of synthetic peptide analogs of the class A amphipathic helix with lipids. Evidence for the snorkel hypothesis. *J. Biol. Chem.* 269:7185–7191.

23. Hevonoja, T., M. O. Pentikäinen, M. T. Hyvönen, P. T. Kovanen, and M. Ala-Korpela. 2000. Structure of low density lipoprotein (LDL) particles: Basis for understanding molecular changes in modified LDL. *Biochim. Biophys. Acta*. 1488:189–210.

24. Sparks, D. L., M. C. Phillips, and S. Lund-Katz. 1992. The conformation of apolipoprotein A-I in discoidal and spherical recombinant high density lipoprotein particles. ^{13}C NMR studies of lysine ionization behavior. *J. Biol. Chem.* 267:25830–25838.

25. Curtiss, L. K., D. J. Bonnet, and K. A. Rye. 2000. The conformation of apolipoprotein A-I in high density lipoproteins is influenced by core lipid composition and particle size: a surface plasmon resonance study. *Biochemistry*. 39:5712–5721.

26. Borhani, D. W., D. P. Rogers, J. A. Engler, and C. G. Brouillette. 1997. Crystal structure of truncated human apolipoprotein A-I suggests a lipid-bound conformation. *Proc. Natl. Acad. Sci. USA*. 94:12291–12296.

27. Brouillette, C. G., G. M. Anantharamaiah, J. A. Engler, and D. W. Borhani. 2001. Structural models of human apolipoprotein A-I: a critical analysis and review. *Biochim. Biophys. Acta*. 1531:4–46.

28. Li, H. H., D. S. Lyles, W. Pan, E. Alexander, M. J. Thomas, and M. G. Sorci-Thomas. 2002. ApoA-I structure on discs and spheres. Variable helix registry and conformational states. *J. Biol. Chem.* 277:39093–39101.

29. Li, H., D. S. Lyles, W. Pan, E. Alexander, M. J. Thomas, and M. G. Sorci-Thomas. 2003. ApoA-I structure on discs and spheres. *J. Biol. Chem.* 277:39093–39101.

30. Phillips, J. C., W. Wriggers, Z. Li, A. Jonas, and K. Schulten. 1997. Predicting the structure of apolipoprotein A-I in reconstituted high density lipoprotein disks. *Biophys. J.* 73:2337–2346.

31. Sheldahl, C., and S. C. Harvey. 1999. Molecular dynamics on a model for nascent high-density lipoprotein: role of salt bridges. *Biophys. J.* 76:1190–1198.

32. Klon, A. E., J. P. Segrest, and S. C. Harvey. 2002. Molecular dynamics simulations on discoidal HDL particles suggest a mechanism for rotation in the apoA-I belt model. *J. Mol. Biol.* 324:703–721.

33. Shih, A. Y., I. G. Denisov, J. C. Phillips, S. G. Sligar, and K. Schulten. 2005. Molecular dynamics simulations of discoidal bilayers assembled from truncated human lipoproteins. *Biophys. J.* 88:548–556.

34. Segrest, J. P., M. K. Jones, A. E. Klon, C. J. Sheldahl, M. Hellinger, H. De Loof, and S. C. Harvey. 1999. A detailed molecular belt model for apolipoprotein A-I in discoidal high density lipoprotein. *J. Biol. Chem.* 274:31755–31758.

35. Davidson, W. S., and G. M. Hilliard. 2003. The spatial organization of apolipoprotein A-I on the edge of discoidal high density lipoprotein particles. A mass spectrometry study. *J. Biol. Chem.* 278:27199–27207.

36. Bhat, S., M. G. Sorci-Thomas, E. T. Alexander, M. P. Samuel, and M. J. Thomas. 2005. Intermolecular contact between globular N-terminal fold and C-terminal domain of apoA-I stabilizes its lipid bound conformation. Studies employing chemical cross-linking and mass spectrometry. *J. Biol. Chem.* 280:33015–33025.

37. Li, L., J. Chen, V. K. Mishra, J. A. Kurtz, D. Cao, A. E. Klon, S. C. Harvey, G. M. Anantharamaiah, and J. P. Segrest. 2004. Double belt structure of discoidal high density lipoproteins: molecular basis for size heterogeneity. *J. Mol. Biol.* 343:1293–1311.

38. Catte, A., J. C. Patterson, M. K. Jones, W. G. Jerome, D. Bashtovyy, Z. Su, F. Gu, J. Chen, M. P. Aliste, S. C. Harvey, L. Li, G. Weinstein, and J. P. Segrest. 2006. Novel changes in discoidal high density lipoprotein morphology: a molecular dynamics study. *Biophys. J.* 90:4345–4360.

39. Shih, A. Y., A. Arkhipov, P. L. Freddolino, and K. Schulten. 2006. Coarse grained protein-lipid model with application to lipoprotein particles. *J. Phys. Chem. B*. 110:3674–3684.

40. Shih, A. Y., P. L. Freddolino, A. Arkhipov, and K. Schulten. 2007. Assembly of lipoprotein particles revealed by coarse-grained molecular dynamics simulations. *J. Struct. Biol.* 157:579–592.

41. Heikelä, M., I. Vattulainen, and M. T. Hyvönen. 2006. Atomistic simulation studies of cholesteryl oleates: model for the core of lipoprotein particles. *Biophys. J.* 90:2247–2257.

42. Lund-Katz, S., L. Liu, S. T. Thuahnai, and M. C. Phillips. 2003. High density lipoprotein structure. *Front. Biosci.* 8:1044–1054.

43. Thompson, M. A. ArgusLab 4.0.1. Planaria Software, Seattle, WA. http://www.arguslab.com.

44. Pitman, M. C., A. Grossfield, F. Suits, and S. E. Feller. 2005. Role of cholesterol and polyunsaturated chains in lipid-protein interactions: molecular dynamics simulation of rhodopsin in a realistic membrane environment. *J. Am. Chem. Soc.* 127:4576–4577.

45. Feller, S. E., D. Yin, R. W. Pastor, and A. D. MacKerell. 1997. Molecular dynamics simulation of unsaturated lipid bilayers at low hydration: parameterization and comparison with diffraction studies. *Biophys. J.* 73:2269–2279.

46. Gao, Q., and B. M. Craven. 1986. Conformation of the oleate chains in crystals of cholesteryl oleate at 123 K. *J. Lipid Res.* 27:1214–1221.

47. Humphrey, W., A. Dalke, and K. Schulten. 1996. VMD: visual molecular dynamics. *J. Mol. Graph.* 14:33–38.

48. Jorgensen, W. L., J. Chandrasekhar, and J. D. Madura. 1983. Comparison of simple potential functions for simulating liquid water. *J. Chem. Phys.* 79:926–935.

49. Marrink, S. J., H. J. Risselada, S. Yefimov, D. P. Tieleman, and A. H. de Vries. 2007. The MARTINI forcefield: coarse grained model for biomolecular simulations. *J. Phys. Chem. B.* 111:7812–7824..

50. Marrink, S. J., A. H. de Vries, and A. E. Mark. 2004. Coarse grained model for semiquantitative lipid simulations. *J. Phys. Chem. B.* 108:750–760.

51. Bond, P. J., and M. S. P. Sansom. 2006. Insertion and assembly of membrane proteins via simulation. *J. Am. Chem. Soc.* 128:2697–2704.

52. Kalé, L., R. Skeel, M. Bhandarkar, R. Brunner, A. Gursoy, N. Krawetz, J. Phillips, A. Shinozaki, K. Varadarajan, and K. Schulten. 1999. NAMD2: greater scalability for parallel molecular dynamics. *J. Comput. Phys.* 151:283–312.

53. MacKerell, A. D., Jr., D. Bashford, M. Bellot, R. L. Dunbrack Jr., J. Evanseck, M. J. Field, S. Fischer, J. Gao, H. Guo, S. Ha, D. Joseph, L. Kuchnir, K. Kuczera, F. T. K. Lau, C. Mattos, S. Michnick, T. Ngo, D. T. Nguyen, B. Prodhom, W. E. Reiher III, B. Roux, M. Schlenkrich, J. Smith, R. Stote, J. Straub, M. Watanabe, J. Wiorkiewicz-Kuczera, D. Yin, and M. Karplus. 1998. All-atom empirical potential for molecular modeling and dynamics studies of proteins. *J. Phys. Chem. B.* 102: 3586–3616.

54. Brooks, B. R., R. E. Bruccoleri, B. D. Olafson, D. J. States, S. Swaminathan, and M. Karplus. 1983. CHARMM: a program for macromolecular energy, minimization and dynamics calculations. *J. Comput. Chem.* 4:187–217.

55. Schlenkrich, M., J. Brickmann, A. D. MacKerell Jr., and M. Karplus. 1996. Empirical potential energy function for phospholipids: criteria for parameter optimization and applications. *In* Biological Membranes: A Molecular Perspective from Computation and Experiment. K. M. Merz and B. Roux, editors. Birkhäuser, Boston. 31–81.

56. Patra, M., and M. Karttunen. 2004. Systematic comparison of force fields for microscopic simulations of NaCl in aqueous solutions: diffusion, free energy of hydration and structural properties. *J. Comput. Chem.* 25:678–689.

57. Berendsen, H. J. C., J. P. M. Postma, W. F. van Gunsteren, A. DiNola, and J. R. Haak. 1984. Molecular dynamics with coupling to an external bath. *J. Chem. Phys.* 81:3684–3690.

58. Darden, T., D. York, and L. Pedersen. 1993. Particle mesh Ewald: An N-log(N) method for Ewald sums in large systems. *J. Chem. Phys.* 98:10089–10092.

59. Lindahl, E., B. Hess, and D. van der Spoel. 2001. GROMACS 3.0: A package for molecular simulation and trajectory analysis. *J. Mol. Model.* 7:306–317.

60. Alignment to principal axes in VMD from the VMD Script Library. 2002. http://www.ks.uiuc.edu/Research/vmd/script_library/scripts/orient/.

61. Colombo, G., S. J. Marrink, and A. E. Mark. 2003. Simulation of MscL gating in a bilayer under stress. *Biophys. J.* 84:2331–2337.

62. Lide, D. R. 1992. Handbook of Chemistry and Physics, CRC Press, Boca Raton, FL..

63. Segrest, J. P., L. Li, G. M. Anantharamaiaha, S. C. Harvey, K. N. Liadakic, and V. Zannis. 2000. Structure and function of apolipoprotein A-I and high-density lipoprotein. *Curr. Opin. Lipidol.* 11:105–115.

64. Segrest, J. P., S. C. Harvey, and V. Zannis. 2000. Detailed molecular model of apolipoprotein A-I on the surface of high-density lipoproteins and its functional implications. *Trends Cardiovasc. Med.* 10:246–252.

65. Marrink, S. J., E. Lindahl, O. Edholm, and A. E. Mark. 2001. Simulation of the spontaneous aggregation of phospholipids into bilayers. *J. Am. Chem. Soc.* 123:8638–8639.

66. Brunger, A. T., J. Kuriyan, and M. Karplus. 1987. Crystallographic R factor refinement by molecular dynamics. *Science.* 235:458–460.

67. Brunger, A. T., P. D. Adams, G. M. Clore, W. L. DeLano, P. Gros, R. W. Grosse-Kunstleve, J. S. Jiang, J. Kuszewski, M. Nilges, N. S. Pannu, R. J. Read, L. M. Rice, T. Simonson, and G. L. Warren. 1998. Crystallography & NMR system: a new software suite for macromolecular structure determination. *Acta Crystallogr. D Biol. Crystallogr.* 54:905–921.

68. Feig, M., A. D. MacKerell Jr., and C. L. Brooks III. 2003. Force field influence on the observation of π-helical protein structures in molecular dynamics simulations. *J. Phys. Chem. B.* 107:2831–2836.

69. Van Wynsberghe, A., G. Li, and Q. Cui. 2004. Normal-mode analysis suggests protein flexibility modulation throughout RNA polymerase's functional cycle. *Biochemistry.* 43:13083–13096.

70. Bond, P. J., and M. S. P. Sansom. 2003. Membrane protein dynamics versus environment simulations of OmpA in a micelle and in a bilayer. *J. Mol. Biol.* 329:1035–1053.

71. Sparks, D. L., W. S. Davidson, S. Lund-Katz, and M. C. Phillips. 1993. Effect of cholesterol on the charge and structure of apolipoprotein A-I in recombinant high density lipoprotein particles. *J. Biol. Chem.* 268:23250–23257.

72. Klon, A. E., J. P. Segrest, and S. C. Harvey. 2002. Comparative models for human apolipoprotein A-I bound to lipid in discoidal high-density lipoprotein particles. *Biochemistry.* 41:10895–10905.

73. Rye, K. A., K. H. Garrety, and P. J. Barter. 1993. Preparation and characterization of spheroidal, reconstituted high-density lipoproteins with apolipoprotein A-I only or with apolipoprotein A-I and A-II. *Biochim. Biophys. Acta.* 1167:316–325.